Composites Science and Technology 208 (2021) 108733

Contents lists available at ScienceDirect

Composites Science and Technology

journal homepage: http://www.elsevier.com/locate/compscitech

Ultra-low CNTs filled high-performance fast self-healing triboelectric nanogenerators for wearable electronics

Panlei Liu [a], Na Sun [a,**], Yuanyuan Mi [b], Xiaohang Luo [b], Xiaoxiao Dong [b], Jiaye Cai [b], Xilai Jia [c], Melvin A. Ramos [d], Travis Shihao Hu [d], Quan Xu [b,*]

[a] School of Mechanical Engineering, Beijing Institute of Technology, Beijing, 100081, China
[b] State Key Laboratory of Heavy Oil Processing, Beijing Key Laboratory of Biogas Upgrading Utilization, China University of Petroleum, Beijing, 102249, China
[c] School of Materials Science and Engineering, University of Science and Technology, Beijing, 100083, China
[d] Department of Mechanical Engineering, California State University, Los Angeles, CA, 90032, United States

ARTICLE INFO

Keywords:
CNTs
PVA hydrogel
Self-healing
Triboelectric nanogenerator
Wearable electronics

ABSTRACT

Self-healing triboelectric nanogenerators (SH-TENGs) with fast self-healing, high output performance, and wearing comfort have wide and promising applications in wearable electronic devices. This work presents a high-performance hydrogel-based SH-TENG, which consists of a high dielectric triboelectric layer (HDTL), a self-healing hydrogel electrode layer (SHEL), and a physical cross-linking layer (PCLL). Carbon nanotubes (CNTs), obtained by a chemical vapor deposition (CVD) method, were added into polydimethylsiloxane (PDMS) to produce the HDTL. Compared with pure PDMS, the short-circuit transferred charge (44 nC) and the open circuit voltage (132 V) are doubled for PDMS with 0.01 wt% CNTs. Glycerin, polydopamine particles (PDAP) and graphene were added to poly (vinyl alcohol) (PVA) to prepare the self-healing hydrogel electrode layer. SHEL can physically self-heal in ~1 min when exposed to air. The self-healing efficiency reaches up to 98%. The PCLL is made of poly(methylhydrosiloxane) (PMHS) and PDMS. It forms a good physical bond between the hydrophilic hydrogel and hydrophobic PDMS layers. The electric output performance of the SH-TENG can reach 94% of the undamaged one in 1 min. The SH-TENG (6 × 6 cm^2) exhibits good stability and superior electrical performance, enabling it to power 37 LEDs simultaneously.

1. Introduction

In recent years, finding new and alternative energy resources and/or energy conversion methods has received growing research attention fueled by many disadvantages encountered in traditional non-renewable energy technologies. Triboelectrification is a well-known phenomenon that provides innovative possibilities for converting mechanical energy into electrical energy [1]. Based on the combination of the triboelectric effect and electrostatic induction, triboelectric nanogenerator (TENG) is one of the most promising methods for self-powered small electronic devices [2,3], due to its unique properties, such as high output performance, cleanness, sustainability and low-cost. Single electrode mode TENG has wide applications in wearable devices since it is only necessary to connect one electrode to the triboelectric layer, and there is no limit to the other charging surface. Inspired by the biological healing of injury tissues, self-healing mechanism is adopted in TENGs to cope with the damage issues and extend their service life. A few studies have demonstrated the importance to design self-healable TENG, to improve the applicability of TENG on wearable devices and avoid degradation caused by mechanical damage/wear and tear [4,5].

Due to inherent capacitance, usually at the level of several megohms, TENG has a large voltage (i.e., hundreds of volts) and a small current (i.e., at μA level) [6]. The output of TENG needs to be further improved to realize commercialization. The improvement of the output performance of TENG mainly depends on the effective contact area of the triboelectric layer and the surface charge density. Because the material of the triboelectric layer is usually made of polymer, increasing the dielectric properties of the polymers is an effective way to increase the surface charge density. High dielectric constant ceramic particles used as a reinforcing phase were added to the polymer to improve the dielectric properties. However, the amount of reinforcements in high dielectric constant composites is usually high (10–30 wt%) [7], which

* Corresponding author.
** Corresponding author.
E-mail addresses: nsun@bit.edu.cn (N. Sun), xuquan@cup.edu.cn (Q. Xu).

https://doi.org/10.1016/j.compscitech.2021.108733
Received 14 November 2020; Received in revised form 5 January 2021; Accepted 12 February 2021
Available online 5 March 2021

significantly reduces the flexibility of the polymer substrate. It has been shown that adding conductive particles can greatly reduce the addition amount (1–5 wt%) [8,9] and achieve excellent dielectric properties [10]. Carbon nanotubes (CNTs) as slender one-dimensional structure with high aspect ratio can easily form conductive paths in the polymer matrix and effectively improve the dielectric properties of materials. Therefore, they are commonly chosen as the reinforcing phase to improve the electric output performance of TENGs.

There are three major types of SH-TENG including: self-healing electrode layer SH-TENG [11,12], self-healing triboelectric layer SH-TENG [13,14], and entirely self-healable SH-TENG [15,16]. Guan et al. [11] [[,12] [][][] explored two different types of SH-TENGs. One had a self-healing hydrogel electrode and a silicone rubber triboelectric layer that could be recovered under near-infrared (NIR) light for 1 min or water spraying at 25 °C for 5 min. The other used an epoxy resin-based polysulfide elastomer as a self-healing electrode layer that could be restored at temperatures above 130 °C. Sun et al. [13] reported an SH-TENG with a self-healing triboelectric layer, which required 12h to recover from damage. Dynamic imine bonds were introduced in PDMS networks for repairing the mechanical damages. Deng et al. [14] used a dynamic disulfide bond-based vitrimer elastomer as a self-healing triboelectric layer. At 65 °C, the self-healing time was 4h. In addition, Chen et al. [15] used viscoelastic polymer-Silly Putty as electrification material, and CNTs filled composite (CNT-putty) as electrode material in preparation of an entirely SH-TENG. The self-healing time was demonstrated to be 3min. Lai et al. [16] prepared an entirely SH-TENG, consisting of a metal-coordinated polymer triboelectrically charged layer and a hydrogen-bonded ionic gel electrode layer. Paraffin wax was used as an intermediate layer between them. The self-healing time was reported as 30 min. Although researchers have explored different types of self-healing TENGs, they are restricted and suffer from specific external conditions, a long self-healing time to achieve self-healing, low adhesion of the triboelectric layers to the electrode layers, complex preparation processes and costly materials.

Herein, we present a high-performance hydrogel-based fast SH-TENG, which recovers without external stimulation, and the self-healing efficiency can reach up 98% in ~1 min in air. The preparation process is simple, and free from complicated reaction conditions. Adding ultra-low CNTs (0.01 wt%) to the HDTL effectively improves the output performance of TENG. The PCLL achieves a good physical bond between the hydrophilic hydrogel and the hydrophobic PDMS, effectively solving the problem of low adhesion problem. The prepared SH-TENG (6 × 6 cm^2) has good stability and excellent electrical performance, enabling it to power 37 LEDs simultaneously. It features short self-healing time, high output performance, and good combination between layers. These attributes make them more adaptable to the changing environments, which help to realize commercialization of flexible and wearable electronic devices.

2. Results and discussion

2.1. SHEL

Self-healing stems from a molecular re-alignment and reassembly process. Unstable bonds play a critical role, which allows rapid bond breakage, reconstruction and structural rearrangement. Compared with covalent bonds, the association or dissociation of hydrogen bonds that occur spontaneously at ambient conditions provides opportunities to develop excellent self-healing materials [17]. To prepare electrode materials with both self-healing and high electrical conductivity, PVA is selected as the matrix. The conductivity can be improved by adding an appropriate amount of graphene. Adding PDAP to the hydrogel improves the mechanical properties of the hydrogel.

Fig. 1a shows a schematic diagram of the internal structure and bonding of a conductive self-healing hydrogel. PDAP contains various functional groups, such as amines and catechol, which can be used as both the chemical reaction sites or covalent modification and physical cross-linking points to improve the interface interaction between the filler and the matrix. In the matrix, PDAP and PVA molecular chains form hydrogen bonds. Introducing PDAP into the hydrogel not only improve the mechanical properties but also give the hydrogel photothermal effect. The self-healing properties of the prepared hydrogel are attributed to the reversible network, as shown in Fig. 1a. The network consists of two dynamic covalent cross-linking reactions in the hydrogel, namely PVA-borax-PVA [18] and PVA-glycerol-PVA [19]. During the hydrogel cooling process, chitosan-agarose, chitosan-PVA and agarose-PVA form hydrogen bonds. These bonds can effectively inhibit the movement of the PVA chain within a certain range, thereby improving the mechanical stability and tensile strength of the hydrogel [20].

Scanning electron microscope (SEM) is commonly employed for studying the structure of PVA hydrogel networks. However, due to volatilization the presence of water in the gel can affect the scanning electron microscope images under low pressure or vacuum conditions. Fig. 1b shows the SEM images of PVA, PVA/PDAP, and PVA/PDAP/Graphene hydrogels after freeze-drying, specifically pure PVA, PVA/0.16 wt%PDAP and PVA/0.16 wt%PDAP/0.48 wt%graphene. PVA assumes a flocculent structure on the surface and the pores are coarse and uneven, as shown in Fig. 1b (I). In Fig. 1b (II), the addition of PDAP can refine the grains, make the pores more uniform, and improve hydrogel performance. In Fig. 1b (III), the PVA/PDAP/Graphene surface shows denser pores, and network cross-linking can be observed. The regions

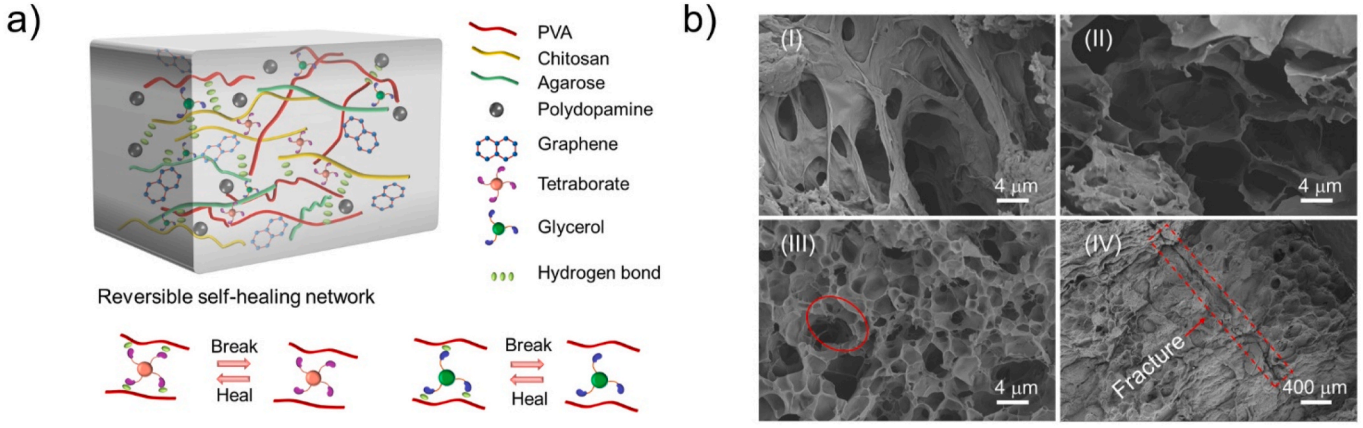

Fig. 1. a) Schematic of the internal structure and bonding of the conductive self-healing hydrogel. b) SEM images of hydrogels with different components, I) PVA, II) PVA/PDAP, III) PVA/PDAP/Graphene, IV) the self-healed interface of PVA/PDAP/Graphene.

marked in the red circles show network cross-linking. For a large view see Fig. S1. The cross-linking of the self-healing fracture surface of the hydrogel is shown in Fig. 1b (IV). After straining or cutting, the damaged hydrogel can repair itself without applying external stimuli.

Fig. 2a shows the Fourier transform infrared spectroscopy (FTIR) spectra of PVA, PVA/PDAP, and PVA/PDAP/Graphene samples. In the FTIR spectra, the –OH stretching band in the PVA/PDAP is located at 3277 cm^{-1}, whereas it shifts to a lower wavenumber compared to that of pristine PVA (3280 cm^{-1}). The -C-OH stretching band also shifts from 1095 cm^{-1} in PVA to 1087 cm^{-1} in the composites. Both of these phenomena indicate that there is hydrogen bonding formed between the hydroxyl groups of PVA and the functional groups of PDAP [21,22]. The –OH stretching band is located at 3298 cm^{-1} for PVA/PDAP/Graphene. This is mainly because the graphene surface can physically absorb gas molecules, such that some functional groups, for example, C–OH and C–O–C exist on the surface.

Fig. 2b shows the tensile stress-strain curves of PVA, PVA/PDAP and PVA/PDAP/Graphene. Compared with the PVA sample the tensile strength of the PVA/PDAP hydrogel sample increased from 66 KPa to 75 KPa by 12%, and the elongation at break increased from 443% to 678% by 53%. The tensile strength of PVA/PDAP/Graphene hydrogel can reach up to 85 KPa. In the hydrogel, PDAP can form hydrogen bonds with the PVA molecular chain (as demonstrated above), therefore improve the mechanical properties of the hydrogel. Graphene molecules can further improve the porous structure of the hydrogel and enhance the mechanical properties of the hydrogels.

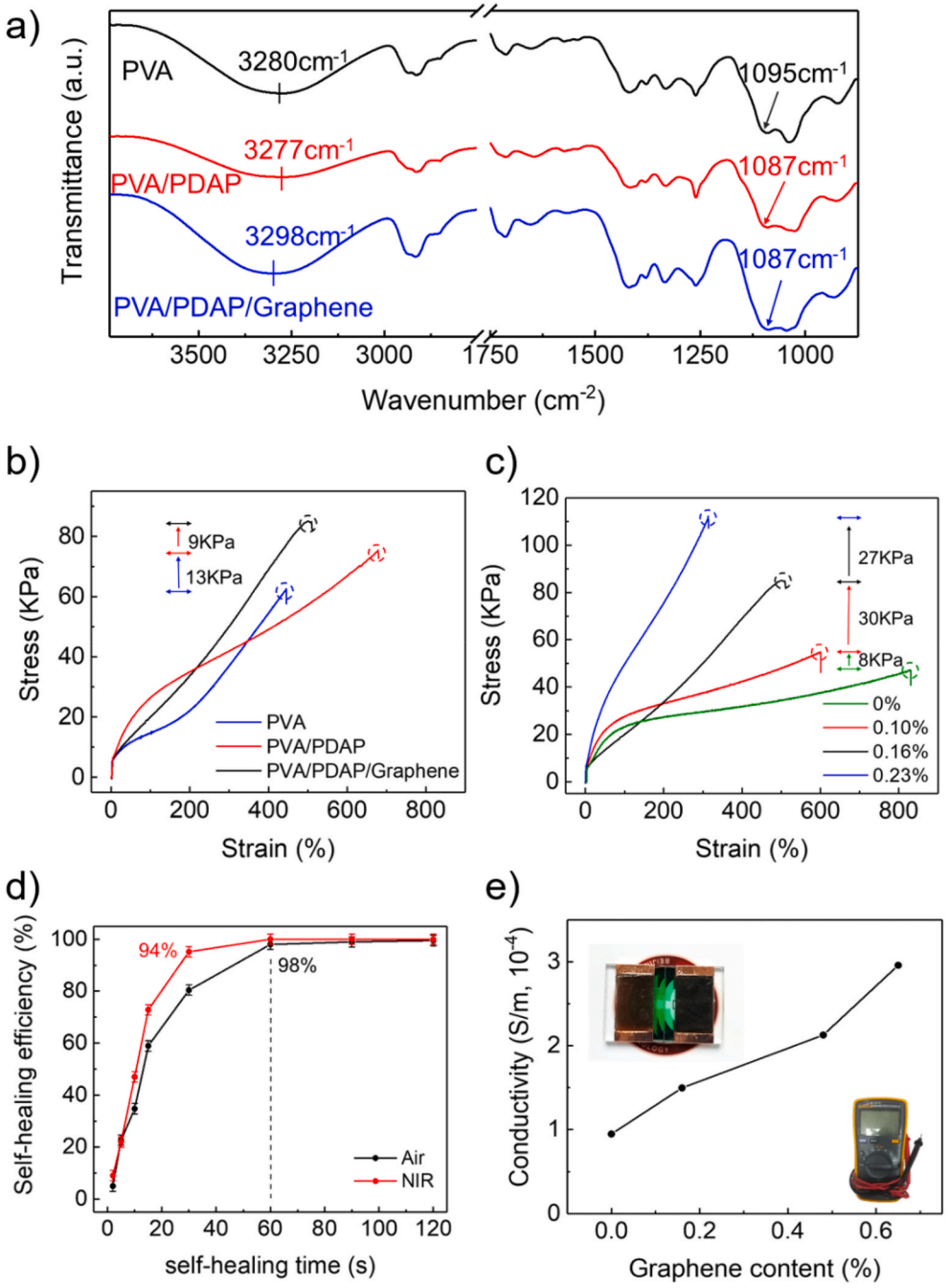

Fig. 2. a) FTIR spectra of the different hydrogels. b) Typical tensile stress-strain curves of different hydrogel samples. c) The tensile stress-strain curves of hydrogels with different PDAP contents. d) Relationship between self-healing efficiency and healing time of the hydrogels in the air and exposed to NIR. e) Electrical conductivity of the hydrogels with different graphene contents.

The tensile stress-strain curves of samples with different PDAP contents are shown in Fig. 2c. The tensile strength increases from 47 KPa to 112 KPa by about 2.4 times, whereas the elongation at break decreases from 830% to 314% by 62% when the PDAP content is increased to 0.23 wt%. This indicates that even adding a small amount of PDAP to the PVA hydrogel can significantly improve the mechanical properties. Since various functional groups are attached to the surface of PDAP, such as catechol and amine, PDAP can bond the hydroxyl group of PVA through hydrogen bonding, thereby increasing the tensile strength [23].

The stretchability of PVA/PDAP/Graphene hydrogel (stretching ratio $\lambda > 4$) is shown in Fig. S2a. The hydrogel ($40 \times 20 \times 3$ mm^3) can be stretched to about 17 cm in length, then after the hydrogel restores to 1.5 times of the original length within 2 min. The photothermal effect of the hydrogel is shown in Fig. S2b, showing the addition of PDAP can improve the photo-thermal properties of the hydrogels. The sample has an ultrafast temperature rise, up to 90 °C in 30s.

The self-healing properties of PVA/PDAP/Graphene hydrogel are shown in Fig. S2d. As shown in the Movie S1, the hydrogel can achieve complete self-healing after 60s. It is worth noting that the hydrogel showed good self-healing performance in air and NIR solutions, as shown in Fig. 2d. The self-healing efficiency can be quantified using the recovery of tensile stress, according to the following equation:

$$\eta = \delta_1/\delta_0 \tag{1}$$

where η designates the self-healing efficiency of the hydrogels, δ_0 and δ_1 are the tensile stresses before and after the hydrogels undergoes self-healing, respectively. Repeat the tests more than 3 times for the same samples. In air, after 60s of healing, the PVA/PDAP/Graphene hydrogel can reach up to 98% healing efficiency. After NIR irradiation, the PVA/PDAP/Graphene hydrogel can reach up to 94% healing efficiency after 30s of healing.

The PVA/PDAP/Graphene hydrogel showed high conductivity, and the hydrogel can illuminate a LED bulb with a constant current in a closed loop. After the first cut, the circuit was disconnected (current = 0 mA) as indicated by the bulb. Then the two fractured hydrogel surfaces were immediately brought together and contacted each other. After 60s of self-healing in situ, the circuit restored its initial current value, and the LED was illuminated again without a significant decrease in brightness. This proves the exceptional self-restoring capability of the prepared conductive hydrogel network (Fig. S3a) [24]. It is shown that graphene can effectively improve the conductivity of the hydrogels. The conductivity was doubled by adding small amount of graphene (0.48 wt %), as shown in Fig. 2e.

2.2. HDTL

To prepare a triboelectric layer material with high dielectric properties, PDMS was selected as the matrix, and carbon nanotubes were well-dispersed as the reinforcing phase to improve the dielectric properties of the materials. Under the effect of van der Waals force, CNTs tend to form clusters and bundles [25]. It is difficult to achieve uniform dispersion of CNTs in conventional ways. Using well-dispersed CNTs as the reinforcing phase can effectively improve the dispersion of CNTs in the matrix. Fig. 3a (I)-(IV) show the SEM images of the cross-sections of the CNTs/PDMS films. The arrows point to the CNTs, and the rest is the PDMS matrix. As shown in Fig. 3a, with the increase of CNTs content, the distribution of CNTs becomes relatively clustered.

Adding CNTs to the PDMS matrix can improve the dielectric properties of the material. Thereby increasing the surface charge density of the triboelectric layer and increasing the TENG output performance. The dielectric constant of the CNTs/PDMS composite film is defined as follows:

$$\varepsilon_r = \frac{C \cdot d}{A \cdot \varepsilon_0} \tag{2}$$

where C denotes the capacitance of the composite film, d represents the

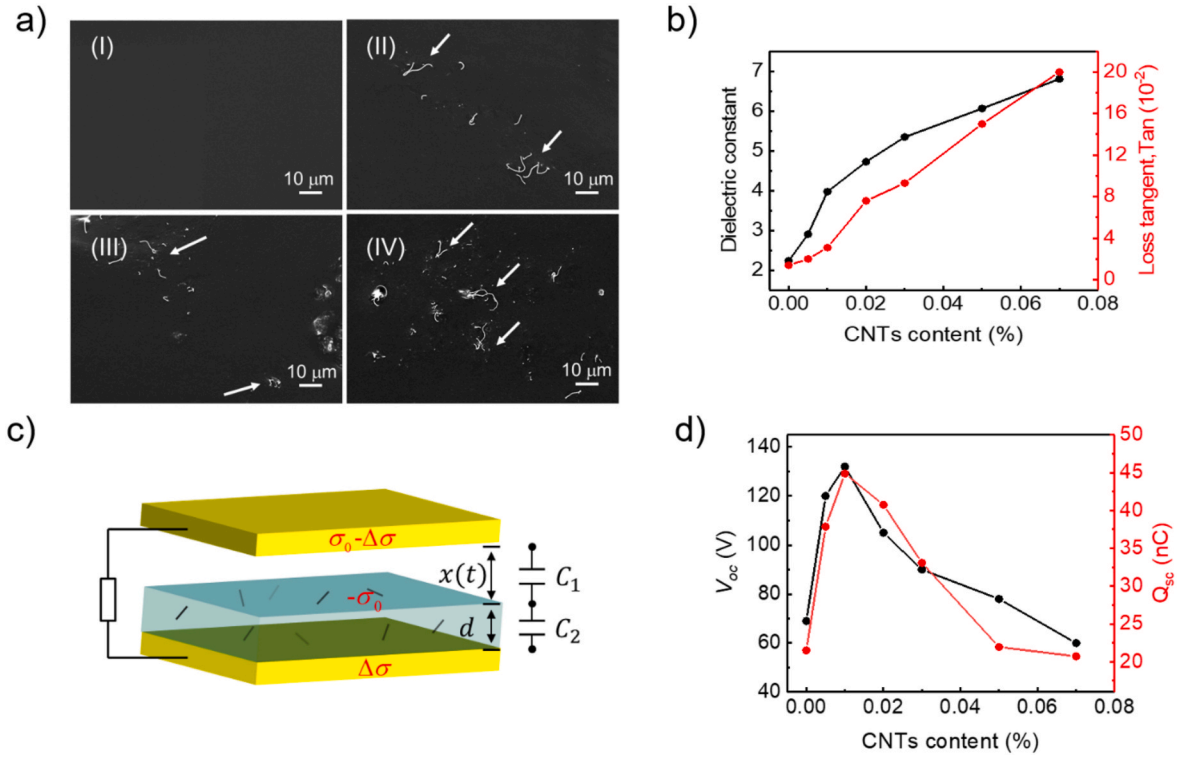

Fig. 3. a) SEM images of the cross-sections of CNTs/PDMS films with different CNTs contents, I) 0%, II) 0.02%, III) 0.05%, IV) 0.07%. b) Dielectric properties of CNTs/PDMS composite films with different amounts of CNTs fillers. c) Schematic showing the contact separation principle. d) The electrical output performance of CNTs/PDMS composite films with different CNTs contents.

thickness of the film, A represents the area of the electrode, ε_0 represents the dielectric constant of the vacuum, respectively. The C and loss tangent D were measured with an Impedance analyzer (1 MHz). The results of dielectric constant and loss tangent are shown in Fig. 3b. As the content of CNTs is increased, the dielectric constant and loss tangent show an increasing trend. When the content of CNTs is less than 0.02%, the growth rate of the dielectric constant is higher than the loss. When the content of CNTs is increased to 0.07%, the dielectric constant and loss tangent are 6.8 and 0.20, respectively. According to the percolation theory, CNTs are conductive phases, while PDMS is the low-loss electrical potential barrier. The CNTs are separated by thin barriers of PDMS regions, and the adjacent nanotubes form nanocapacitors. Therefore, the dielectric constant and loss increase as the content of CNTs increases [26,27].

The electrical output performance of CNTs/PDMS films was tested by contact separation mode. The principle of contact separation is shown in Fig. 3c. According to previous work [28–30], the output voltage V can be expressed by

$$V = \frac{(\sigma_0 - \Delta\sigma)\cdot x(t)}{\varepsilon_0} - \frac{\Delta\sigma \cdot d}{\varepsilon_0 \varepsilon_r} \tag{3}$$

where σ_0, $\Delta\sigma$, $x(t)$, t are the triboelectric charge density on the composite film, the transferred charge density on the Cu electrode in the stage, the interlayer distance and time, respectively.

At the open-circuit (OC) condition, there is no charge transfer, which means $\Delta\sigma$ becomes 0. Therefore, the open-circuit voltage is given by

$$V_\alpha = \frac{\sigma_0 \cdot x(t)}{\varepsilon_0} \tag{4}$$

The theory of TENG is derived from Maxwell's equations, and its working principle is the conjugation of contact electrification and electrostatic induction. Contact electrification provides static polarized charges and electrostatic induction is the main mechanism for converting mechanical energy into electrical energy. TENG has inherent capacity characteristics [31], since the fundamental device based on electrostatics is a capacitor. The contact separation model can be considered as a flat-panel capacitor. Due to the characteristics of electret, the negative charges on the surface of CNTs/PDMS derived from interfacial friction remain constant, so two flat-panel capacitors should be included. The fixed capacitor is composed of the upper Cu electrode and the surface of electret film, which is separated by a dielectric air with a capacitance of $C_1 = \frac{\varepsilon_0 S}{x}$ (S represents the contact area). The other capacitor consists of the bottom Cu electrode and the surface of electret film separated by the CNTs/PDMS composite film with a capacitance of$C_2 = \frac{\varepsilon_r S}{x}$. The characteristics of capacitance are very important for the energy storage, which determine the maximum charge density σ_0 on the film surface. Improving the dielectric constant of the CNTs/PDMS composite film will help to increase the surface charge density of the triboelectric layer, and in turn increase the output of TENG.

Fig. 3d and Fig. S3b shows the effect of the CNTs concentration on electrical output performance. When the CNTs concentration is 0.01 wt %, the short-circuit transferred charge (Q_{sc}) achieves 44 nC and the open circuit voltage (V_{oc}) becomes 132V. Both reach the maximum values. Compared to the output performance of pure PDMS film, which is 22 nC (Q_{sc}) and 69 V (V_{oc}), the Q_{sc} of 0.01 wt% CNTs/PDMS film is improved by 100% and the V_{oc} improved by 91%. With the continuous increase of CNT content, both Q_{sc} and V_{oc} show a downward trend. The output performance of 0.07 wt% CNTs/PDMS film is 20 nC and 65 V.

Eq. (2) implies that the dielectric constant is directly proportional to the capacitance. However, the loss tangent refers to the leakage current during charge storage. The larger the loss tangent the greater the leakage current during charge storage, which does not contribute to the charge storage. Thus, the capacitance is influenced by the dielectric constant and dielectric loss. When the concentration of CNTs is 0.01 wt%, the dielectric constant increased rapidly, and the dielectric loss was at a relatively small value. Therefore, the output of the composite film was relatively high. When the CNT content is greater than 0.07 wt%, as the CNT content increases, the growth rate of dielectric loss is greater than that of the dielectric constant, resulting in a decrease in output performance.

2.3. The SH-TENG

In the SH-TENG, the PVA/PDAP/Graphene conductive hydrogel is used as the SHEL to transport charge, the CNT/PDMS (0.01 wt%) composite film is used as the HDTL. By adding a cross-linking agent, a good physical bond between the hydrophilic hydrogel and the hydrophobic PDMS is achieved, as shown in Fig. S2c. Figure S2c (I) shows PDMS and hydrogel are easily peeled off and are almost incompatible without applying the cross-linking agent. Adding PMHS to PDMS can effectively improve the adhesion of PDMS and achieve hydrogel and PDMS adherence.

The working principle of SH-TENG couples contact electrification and electrostatic induction, as schematically shown in Fig. 4. TENG is driven by physical contact with the skin. Once the skin contacts the TENG composite film, HDTL becomes negatively charged, whereas the skin is positively charged. Since the two opposite charges coincide on the same plane, there is no electrical potential difference between the two surfaces. When the skin is separated from the composite film, the positive charges are induced in the SHEL (conductive hydrogel) and electrons will flow from the SHEL to the ground through an external circuit. Then an electrical signal is obtained. When the skin is far enough from the film, the positive charges induced on SHEL will completely balance the negative charges on the HDTL and the flow of electrons cease. When the skin is reattached to the film, the electrons will flow in the opposite direction forming an alternating current in the circle.

Fig. 5 shows the schematic diagram of the self-healing mechanism of SH-TENG. Due to the remarkable self-healing properties, the hydrogel electrode layer can quickly heal in air after being damaged ensuring the contact area remains intact. The SH-TENG achieves self-healing under the action of the hydrogel electrode, as shown in Fig. 5a and b. Fig. 5c shows the electrical output performance of SH-TENG (2.5 × 2.5 cm^2) before mechanical damage and after healing. The Q_{sc} and V_{oc} before damage are 18 nC and 54 V, respectively. After 1 min of self-healing, the Q_{sc} and V_{oc} become 17 nC and 50 V, and the output performance can reach 94% and 92% of the undamaged one, respectively. The self-powered system SH-TENG (6 × 6 cm^2) can collect sufficient mechanical energy from human body movement to light up 37 LEDs, making it feasible to power many soft and flexible devices, as shown in Fig. 5d and the Movie S2. The as prepared SH-TENGs show promising results as robust power sources for flexible and wearable electronic devices.

3. Conclusions

We have successfully demonstrated a hydrogel-based high-performance self-healing TENG (SH-TENG). It consists of a high dielectric triboelectric layer (HDTL), a fast self-healing electrode layer (SHEL) and a physical cross-linking layer (PCLL). Adding 0.01 wt% fully dispersed CNTs can effectively increase the dielectric constant of PDMS, thereby increasing the surface charge density. The electrical output performance of the CNT modified PDMS can be doubled, and the V_{oc} and Q_{sc} can reach ~132V and ~44 nC, respectively. After completely cut open or damaged, SHEL can self-heal in ~1 min when exposed to the air. The self-healing efficiency reaches up to 98%. By adding a cross-linking agent, a robust physical bond between the hydrophilic hydrogel and hydrophobic PDMS is achieved. The SH-TENG with hydrogel electrode can self-heal in a timely fashion, whose output performance can reach 94% of the undamaged sample in about 1 min. The SH-TENG (6 × 6 cm^2) exhibits good stability and excellent electrical performance, enabling it to light up 37 LEDs simultaneously.

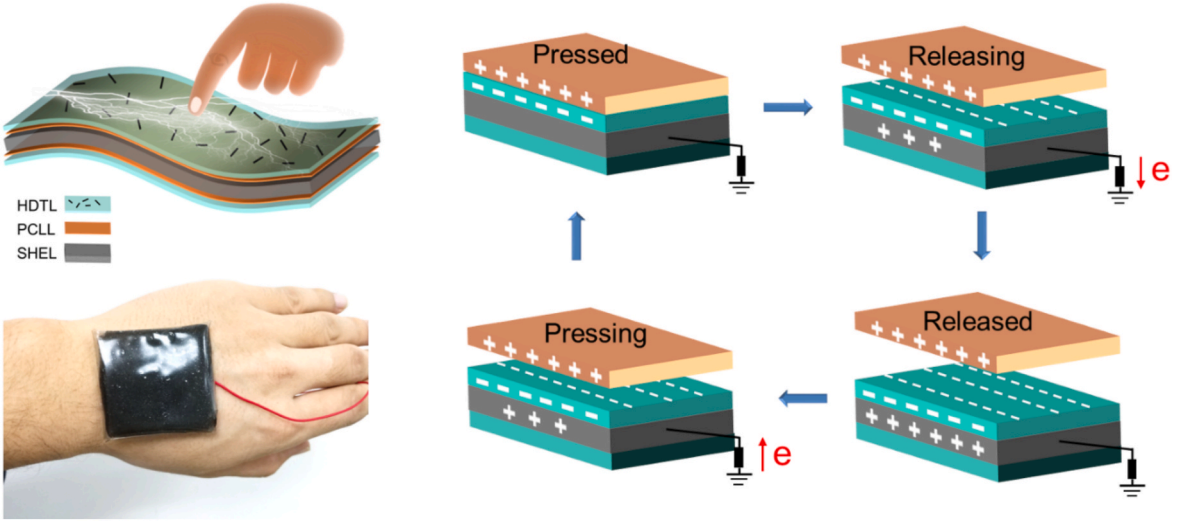

Fig. 4. The picture of SH-TENG attached to the back of a human hand, and the schematics of the working principle.

4. Experimental section

Materials. PVA (degree of polymerization: 2699) was purchased from Anhui Wanwei Group Co., Ltd. Chitosan (BR) was purchased from Sinopharm Chemical Reagent Co. Ltd. PDMS, Sylgard 184 was purchased from Dow Corning Inc. Poly(methylhydrosiloxane) (PMHS, 15–40 mPa s (20 °C)) and chlorotrimethylsilane (TMCS) were purchased from Shanghai Aladdin Biochemical Technology Co. Ltd. Carbon nanotubes (CNTs) were prepared in a fluidized bed reactor by the CVD method using a vermiculite-supported catalyst. Graphene (SE4532, single layer, thickness: ~2 nm, 100–500 m^2/g) was purchased from Changzhou Sixth Element Materials Technology Co. Ltd. Dopamine hydrochloric acid (DA·HCl, 99%) and agarose (BR) were purchased from Shandong West Chemical Co. Ltd. Sodium tetraborate decahydrate ($Na_2B_4O_7H_2O$, 99.5%) was purchased from Tianjin Guangfu Technology Development Co. Ltd.

Preparation of polydopamine particles (PDAP). NH_3H_2O (3.75 mL, 25%), ethanol (60 mL, 99.7%) and deionized water (135 mL) were added to a 250 mL three-necked flask, and the mixture was magnetically stirred at temperature of 30 °C for 30 min. DA·HCl (0.75 g) was added to 15 mL of deionized water, and the obtained aqueous solution was transferred to the previous mixture, which was magnetically stirred at room temperature for another 24 h. Then, PDAPs were collected by centrifugation and washed 3 times with deionized water.

Fabrication of the SHEL. Fig. S4a shows the fabrication process of the self-healing hydrogel. PVA (2.5 g), PDAPs (0.05 g), graphene (0.15 g), glycerin (0.5 mL, 99%) were mixed with 12.5 mL of deionized water. The solution was oil-bathed at 98 °C and magnetically stirred for 2 h to form a gel-like mixture. Then agarose (0.125 g), chitosan (0.125 g), and $Na_2B_4O_7H_2O$ solution (15 ml, 0.04 M) were added directly to the gel-like mixture, which was then oil-bathed at 98 °C for another 1 h. Next, the mixture was put in a petri dish, cover with plastic wrap and pressed by a 2 kg weight for 3 h to remove air bubbles from the gel and the conductive gel material was obtained. The material was shaped to the desired geometry (e.g., 20 × 20 × 3 mm^3). Table 1 lists the chemical compositions of different self-healing hydrogels.

Preparation of CNTs. CNTs were prepared in a fluidized bed reactor using a CVD method [32]. Then they were alternately washed with HCl and HF at 80 °C for 2 h to remove the catalyst and dispersed in ethanol (10 mg/mL) for later use.

Fabrication of HDTL. Fig. S4b schematically illustrates the fabrication process of the CNTs/PDMS composite film. A glass piece was placed in a Petri dish. The TMCS was added into the dish until the glass was immersed. The dish was placed in a fume hood for 15 min. Then it was washed with deionized water and absolute ethanol, sequentially. After that, the dish was blown dry with compressed air.

At room temperature, the PDMS base resin (4g) was mixed with 20 mL chloroform for 30 min using a magnetic stirrer to dilute the PDMS. Then according to the mass fraction (0.005%, 0.01%, 0.02%, 0.03%, 0.05% and 0.07%), different amounts of CNTs uniformly dispersed ethanol solution were added to the diluted PDMS. The mixture was magnetically stirred to evaporate the solvents at 75 °C for 2–3 h. It was then placed in a blast-drying oven at 80 °C for 1 h to ensure complete evaporation of the solvent. Next, the curing agent (0.4 g) was added in with a weight ratio of 1:10. After stirring for 15 min with a glass rod, the mixture was vacuumed to remove air bubbles. Then the PDMS mixture with a thickness of 100 μm (see Fig. S5b) was uniformly spin-coated on the glass at 700 rpm for 20s. Subsequently, the glass was placed in a blast-drying oven at 120 °C for 30 min to cure the film. After that, the film was cooled to room temperature and peeled off from the glass.

Fabrication of the SH-TENG. The PMDS base resin and curing agent were mixed with a weight ratio of 10:1. The mixture was coated on a 65.0 × 65.0 mm^2 mold up to a thickness of ~2.0 mm. Then a piece of conductive hydrogel (60.0 × 60.0 mm^2) was placed on top of the cured PDMS. Next, another layer of CNTs/PDMS composite film with a thickness of about 100 μm was coated on the hydrogel to form a device with a sandwich structure. To achieve a good adherence of hydrogel and PDMS, the composite film was coated with a hydrogel crosslinking agent. The crosslinking agent consisted of PDMS and PMHS. The PDMS base resin (2g) and curing agent (0.2g) were added with a weight ratio of 10:1. Then, PMHS (0.1g) was mixed and stirred with a glass rod for 15 min to make the hydrogel crosslinking agent. The schematic diagram of SH-TENG is shown in Fig. 4.

Characterization. Scanning electron microscope (SEM) images were taken with a SU8220 scanning electron microscope (Hitachi High-tech Co., Ltd, Japan) to characterize the distribution of CNTs and the internal structure of hydrogels. The surfaces of the samples were sprayed with gold. The test voltage was 5 kV. Tensile and compression tests were carried out using a universal tensile tester (HD-B609A-S, Haida International Instruments Co., Ltd, China) to characterize the mechanical properties and self-healing properties of the hydrogels. The speed of tensile tests was 50 mm/min. Based on the GB/T528 standard, the hydrogel samples were made into dumbbell-shaped specimens for tensile tests. Fourier transform infrared spectroscopy (FTIR) was conducted on a Bruker Tensor 27 spectrophotometer (Bruker Optics Co. Ltd, Germany) to analyze the spectra of the hydrogels. The photothermal effect of PDAPs was tested with an Infrared Thermal Imager (Fotric 225s, Shanghai Reimage Technology Co., Ltd, China) under the NIR laser of

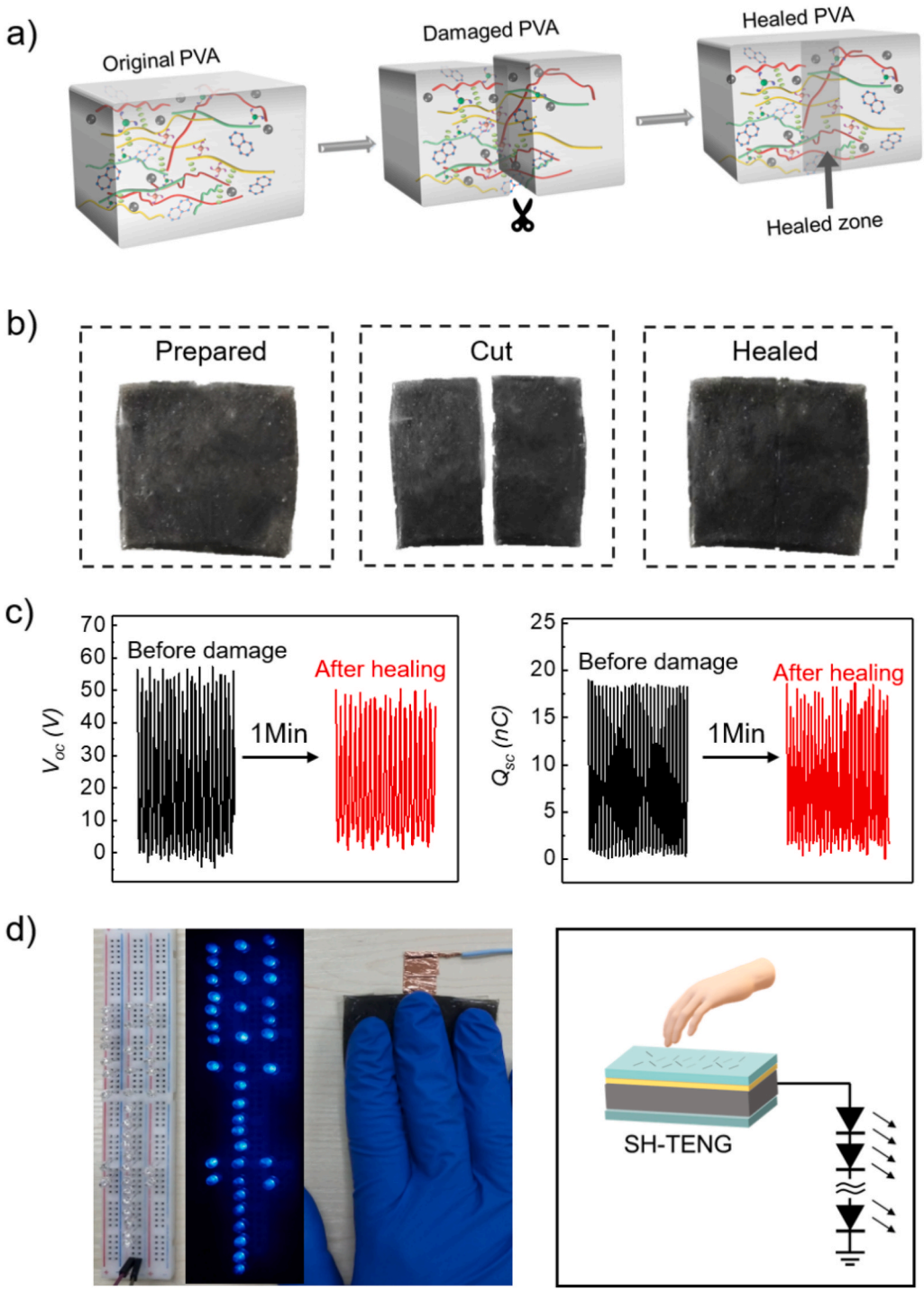

Fig. 5. Schematic of the self-healing mechanism of the SH-TENG. a) Schematic illustration of the PVA hydrogel self-healing mechanism - breaking and reforming of hydrogen bonding. b) The pictures showing as prepared, breakage and healing of SH-TENG samples. c) The electrical output performance (V_{oc} and Q_{sc}) of SH-TENG (2.5 × 2.5 cm^2) before mechanical damage and after healing. d) The picture of the SH-TENG lighting 37 LEDs.

808 nm light. The dielectric constant and loss tangent were measured with an impedance analyzer (4285A, Agilent Technology Co., Ltd, USA) to characterize the dielectric properties of the materials. The test frequency was kept 1 MHz. The thickness of the CNTs/PDMS films was measured by a 3D Profilometer (Nanomap-D, Aep Technology Inc., USA). Each of the same samples was repeated more than 3 times.

For the self-healing tests of conductive hydrogels, the self-healing properties were manifested by the self-healing efficiency defined by Eq. (1).

For conductivity tests, the hydrogels were pressed into a 30 × 20 × 5 mm^3 block. Copper foils were attached to both ends of the block. The relative resistance of the hydrogel was calculated by measuring the resistance between the copper foils by a multimeter. The conductivity of hydrogels was calculated as follows:

$$k = \frac{1}{\rho} = \frac{1}{R} \times \frac{L}{S} \tag{5}$$

Where k represents conductivity, ρ represents resistivity, and R, L and S represent the resistance, the length and the cross-sectional area of

Table 1
Chemical compositions of different conductive hydrogels (wt.%).

No.	PVA	PDAP	Graphene	Sodium borate	Chitosan	Agarose	Glycerin	DI-water	Total
1	8.13	0	0	0.74	0.41	0.41	1.6	Balance	100
2	8.12	0.16	0	0.74	0.41	0.41	1.6	Balance	100
3	8.09	0	0.49	0.74	0.40	0.40	1.6	Balance	100
4	8.08	0.10	0.48	0.74	0.40	0.40	1.6	Balance	100
5	8.08	0.16	0.48	0.74	0.40	0.40	1.6	Balance	100
6	8.07	0.23	0.48	0.74	0.40	0.40	1.6	Balance	100
7	8.10	0.16	0.16	0.74	0.41	0.41	1.6	Balance	100
8	8.06	0.16	0.65	0.74	0.40	0.40	1.6	Balance	100

conductive hydrogel samples, respectively.

The electrical performance of HDTL was obtained using an electrical property test platform in contact separation mode. The driving frequency was 8 Hz and the maximum separation was 10 mm, as shown in Fig. S5a. The values of V_{oc} and Q_{sc} were measured by a programmable electrometer (Keithley 6514). The structure of TENG is consisted of two plates (25×25 mm^2), with an acrylic plate as the substrate material. On one substrate copper foil was attached to the surface as an electrode, which was also as one of the triboelectric layers. The other copper foil, as an electrode, was sandwiched between the substrate and the CNTs/PDMS film. Copper foils were connected to the two terminals of Keithley 6514 to form a test circuit, as shown in Figure S5c (I).

The electrical output performance of SH-TENG was tested in single electrode mode. The SH-TENG was attached to an acrylic substrate. Copper foil was connected to the hydrogel-TENG to produce electrical signals. Copper foil was also used as another contact material. In the quantitative test, the copper foil was connected to one terminal of a Keithley 6514, and the other terminal of Keithley 6514 was connected to the ground terminal of the socket to form a test circuit, as shown in Figure S5c (II).

Author statement

The authors declare no conflict of interest in this submission. This paper has not been considered elsewhere and all the authors approve this revision.

Quan Xu on behalf of all the authors.

Declaration of competing interest

The authors declare that they have no known competing financial interests or personal relationships that could have appeared to influence the work reported in this paper.

Acknowledgments

The authors would like to thank Prof. Guoxin Xie, Prof. Qian Zhao and Prof. Chi Zhang for the help of dielectric constant and electrical output performance measurement. This work was financially supported by the National Natural Science Foundation of China (Grant Nos. 51105223 and 51735001,51875577), Science Foundation of China University of Petroleum (No. 2462020YXZZ018, 2462019QNXZ02), the Tribology Science Fund of State Key Laboratory of Tribology (SKLTKF15A02), and the U.S. National Science Foundation (Award No. 2004251).

Appendix A. Supplementary data

Supplementary data to this article can be found online at https://doi.org/10.1016/j.compscitech.2021.108733.

References

[1] J. Henniker, Triboelectricity in polymers, Nature 196 (4853) (1962), 474-474.
[2] Z.L. Wang, W.Z. Wu, Nanotechnology-enabled energy harvesting for self-powered micro-/nanosystems, Angew. Chem. Int. Ed. 51 (47) (2013) 11700–11721.
[3] H. Guo, J. Wan, H.X. Wu, H.B. Wang, L.M. Miao, Y. Song, H.T. Chen, M.D. Han, H. X. Zhang, Self-powered multifunctional electronic skin for a smart anti-counterfeiting signature system, ACS Appl. Mater. Interfaces 12 (19) (2020) 22357–22364.
[4] N. Luo, Y.G. Feng, D.A. Wang, Y.B. Zheng, Q. Ye, F. Zhou, W.M. Liu, New self-healing triboelectric nanogenerator based on simultaneous repair friction layer and conductive layer, ACS Appl. Mater. Interfaces 12 (27) (2020) 30390–30398.
[5] H.M. Chen, J.J. Koh, M.M. Liu, P.J. Li, X.T. Fan, S.Q. Liu, J.C.C. Yeo, Y.J. Tan, B.C. K. Tee, C.B. He, Super tough and self-healable poly(dimethylsiloxane) elastomer via hydrogen bonding association and its applications as triboelectric nanogenerators, ACS Appl. Mater. Interfaces 12 (28) (2020) 31975–31983.
[6] X.L. Cheng, W. Tang, Y. Song, H.T. Chen, H.X. Zhang, Z.L. Wang, Power management and effective energy storage of pulsed output from triboelectric nanogenerator, Nano Energy 61 (2019) 517–532.
[7] C.W. Deng, N. Sun, P.L. Liu, H.Y. Zhao, X.L. Wang, Influence of the adhesion and dielectric properties on the triboelectric performance of PDMS-x$BaTiO_3$ composite films, Func. Mater. 51 (6) (2020), 06007-06011. (in Chinese).
[8] Z. Zhang, Y. Chen, D.K. Debeli, J.S. Guo, Facile method and novel dielectric material using a nanoparticle-doped thermoplastic elastomer composite fabric for triboelectric nanogenerator applications, ACS Appl. Mater. Interfaces 10 (15) (2018) 13082–13091.
[9] M.-K. Kim, M.-S. Kim, H.-B. Kwon, S.-E. Jo, Y.-J. Kim, Wearable triboelectric nanogenerator using a plasma-etched PDMS–CNT composite for a physical activity sensor, RSC Adv. 7 (76) (2017) 48368–48373.
[10] S. Guan, S. Song, H. Li, G. Mo, S. Zhao, L. Guo, Development of carboxyl-functionalized multi-walled nanotube/polydimethylsiloxane novel polymeric nanodielectric material, Mater. Lett. 216 (2018) 281–286.
[11] Q.B. Guan, G.H. Lin, Y.Z. Gong, J.F. Wang, W.Y. Tan, D.Q. Bao, Y. Liu, Z.W. You, X. H. Sun, Z. Wen, Y. Pan, Highly efficient self-healable and dual responsive hydrogel-based deformable triboelectric nanogenerators for wearable electronics, J. Mater. Chem. A 7 (23) (2019) 13948–13955.
[12] Q. Guan, Y. Dai, Y. Yang, X. Bi, Z. Wen, Y. Pan, Near-infrared irradiation induced remote and efficient self-healable triboelectric nanogenerator for potential implantable electronics, Nano Energy 51 (2018) 333–339.
[13] J. Sun, X. Pu, M. Liu, A. Yu, C. Du, J. Zhai, W. Hu, Z.L. Wang, Self-healable, stretchable, transparent triboelectric nanogenerators as soft power sources, ACS Nano 12 (6) (2018) 6147–6155.
[14] J.N. Deng, X. Kuang, R.Y. Liu, W.B. Ding, A.C. Wang, Y.C. Lai, K. Dong, Z. Wen, Y. X. Wang, L.L. Wang, H.J. Qi, T. Zhang, Z.L. Wang, Vitrimer elastomer-based jigsaw puzzle-like healable triboelectric nanogenerator for self-powered wearable electronics, Adv. Mater. 30 (14) (2018) 1705918.
[15] Y. Chen, X. Pu, M. Liu, S. Kuang, P. Zhang, Q. Hua, Z. Cong, W. Guo, W. Hu, Z. L. Wang, Shape-adaptive, self-healable triboelectric nanogenerator with enhanced performances by soft solid-solid contact electrification, ACS Nano 13 (8) (2019) 8936–8945.
[16] Y.-C. Lai, H.-M. Wu, H.-C. Lin, C.-L. Chang, H.-H. Chou, Y.-C. Hsiao, Y.-C. Wu, Entirely, intrinsically, and autonomously self-Healable, highly transparent, and superstretchable triboelectric nanogenerator for personal power sources and self-powered electronic skins, Adv. Funct. Mater. (2019) 1904626.
[17] M.N. He, X.S. Chen, D.H. Liu, D.C. Wei, Two-dimensional self-healing hydrogen-bond-based supramolecular polymer film, Chin. Chem. Lett. 30 (5) (2019) 961–965.
[18] L.R. He, D. Szopinski, Y. Wu, G.A. Luinstra, P. Theato, Toward self-healing hydrogels using one-pot thiol-ene click and borax-diol chemistry, ACS Macro Lett. 4 (7) (2015) 673–678.
[19] T.Q. Liu, X. Peng, Y.N. Chen, Q.W. Bai, C. Shang, L. Zhang, H.L. Wang, Hydrogen-bonded polymer-small molecule complexes with tunable mechanical properties, Macromol. Rapid Commun. 39 (9) (2018) 1800050.
[20] M. Li, W. Li, W. Cai, X. Zhang, Z. Wang, J. Street, W.-J. Ong, Z. Xia, Q. Xu, A self-healing hydrogel with pressure sensitive photoluminescence for remote force measurement and healing assessment, Mater. Horizons 6 (4) (2019) 703–710.
[21] H.J. Salavagione, G. Martinez, M.A. Gomez, Synthesis of poly(vinyl alcohol)/reduced graphite oxide nanocomposites with improved thermal and electrical properties, J. Mater. Chem. 19 (28) (2009) 5027–5032.
[22] S.Q. Xiong, Y. Wang, J.R. Yu, L. Chen, J. Zhu, Z.M. Hu, Polydopamine particles for next-generation multifunctional biocomposites, J. Mater. Chem. A 2 (20) (2014) 7578–7587.

[23] L. Yang, Z.H. Wang, G.X. Fei, H.S. Xia, Polydopamine particles reinforced poly (vinyl alcohol) hydrogel with NIR light triggered shape memory and self-healing capability, Macromol. Rapid Commun. 38 (23) (2017) 1700421.
[24] Y. Shi, G. Yu, Designing hierarchically nanostructured conductive polymer gels for electrochemical energy storage and conversion, Chem. Mater. 28 (8) (2016) 2466–2477.
[25] P.M. Ajayan, J.M. Tour, Materials science: nanotube composites, Nature 447 (7148) (2007) 1066–1068.
[26] Z.M. Dang, Y.H. Lin, C.W. Nan, Novel ferroelectric polymer composites with high dielectric constants, Adv. Mater. 15 (19) (2003) 1625–1629.
[27] M. Tian, Q. Ma, X.L. Li, L.Q. Zhang, T. Nishi, N.Y. Ning, High performance dielectric composites by latex compounding of graphene oxide-encapsulated carbon nanosphere hybrids with XNBR, J. Mater. Chem. A 2 (29) (2014) 11144–11154.
[28] S.M. Niu, S.H. Wang, L. Lin, Y. Liu, Y.S. Zhou, Y.F. Hu, Z.L. Wang, Theoretical study of contact-mode triboelectric nanogenerators as an effective power source, Energy Environ. Sci. 6 (12) (2013) 3576–3583.
[29] X.M. He, H.Y. Guo, X.L. Yue, J. Gao, Y. Xi, C. Hu, Improving energy conversion efficiency for triboelectric nanogenerator with capacitor structure by maximizing surface charge density, Nanoscale 7 (5) (2015) 1896–1903.
[30] J. Chen, H.Y. Guo, X.M. He, G.L. Liu, Y. Xi, H.F. Shi, C.G. Hu, Enhancing performance of triboelectric nanogenerator by filling high dielectric nanoparticles into sponge PDMS film, ACS Appl. Mater. Interfaces 8 (1) (2016) 736–744.
[31] S.M. Niu, Y. Liu, S.H. Wang, L. Lin, Y.S. Zhou, Y.F. Hu, Z.L. Wang, Theory of sliding-mode triboelectric nanogenerators, Adv. Mater. 25 (43) (2013) 6184–6193.
[32] X. Zhu, L. Han, Y.F. Lu, F. Wei, X.L. Jia, Geometry-induced thermal storage enhancement of shape-stabilized phase change materials based on oriented carbon nanotubes, Appl. Energy 791 (2019) 1105–1113.